Heliyon 10 (2024) e28365

Contents lists available at ScienceDirect

Heliyon

journal homepage: www.cell.com/heliyon

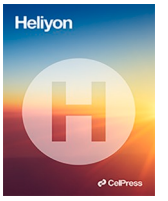

Research article

AURKA knockdown inhibits esophageal squamous cell carcinoma progression through ferroptosis

Yuan Mi [a,1], Liying Chen [b,1], Cong Wang [c], Yuxin Miao [d], Chuntao Song [a], Jie Su [a], Lei Wang [e,*]

[a] Department of Emergency, The Fourth Hospital of Hebei Medical University, Shijiazhuang, 050011, Hebei, China
[b] Department of Physiology, Hebei University of Chinese Medicine, Shijiazhuang, 050200, Hebei, China
[c] Department of Pharmacy, Hebei Medical University, Shijiazhuang, 050017, Hebei, China
[d] Department of Physiology, Hebei Medical University, Shijiazhuang, 050017, Hebei, China
[e] Department of Thoracic Surgery, The Fourth Hospital of Hebei Medical University, Shijiazhuang, 050011, Hebei, China

ARTICLE INFO

Keywords:
Esophageal squamous cell carcinoma (ESCC)
AURKA
Ferroptosis
Progression
Ferrostatin-1 (Fer-1)

ABSTRACT

Aurora kinase A, as a pro-carcinogenic in gastric cancer and glioma kinase, is enhanced in several human tumors. However, it's regulatory mechanism in esophageal squamous cell carcinoma (ESCC) remains unclear. Thus, this study aimed to investigate the expression status, functional roles, and molecular mechanisms of AURKA in ESCC development. AURKA expression was analyzed by the screening of the GEO database and detected using an immunohistochemical method. The biological function of AURKA on ESCC was evaluated in vitro and in vivo. Western blot assay, malondialdehyde (MDA), iron, and glutathione (GSH) kits were utilized to assess changes in ferroptosis. Database analysis results showed that AURKA was a differential gene in ESCC and was highly expressed in human ESCC tissues. Functionally, AURKA knockdown decreased ESCC cell proliferation, invasion, and metastasis both in vitro and in vivo. Moreover, when AURKA was knockdown, cells were more correctly blocked in the G2/M phase, and the ferroptosis-related MDA and Fe increased, whereas the GSH reduced. Consistently, Glutathione peroxidase 4 (GPX4) and solute carrier family 7a member 11 (SLC7A11) expression were downregulated by AURKA knockdown. However, ferroptosis inhibitor partially restore ESCC cell proliferation, invasion, and metastasis caused by AURKA knockdown. AURKA knockdown enhances ferroptosis and acts against cancer progression in ESCC. AURKA acts as a tumor-promoting gene and may serve as potential target for ESCC treatment.

1. Introduction

Esophageal cancer is a highly prevalent cancer with a high fatality rate, with more than 572,000 new cases and 508,000 deaths each year [1]. Esophageal cancer has two main pathological subtypes, esophageal squamous cell carcinoma (ESCC) and esophageal adenocarcinoma (EAC), which are geographically and epidemiologically distinct. China, as a high-risk esophageal cancer area, more

* Corresponding author.
E-mail addresses: miyuan_medicine@163.com (Y. Mi), liyingchen2016@126.com (L. Chen), 465806841@qq.com (C. Wang), 2391250172@qq.com (Y. Miao), 378224197@qq.com (C. Song), 79234920@qq.com (J. Su), yuankundu@163.com, yuankundu@163.com (L. Wang).
[1] These authors have contributed equally to this work and share first authorship.

https://doi.org/10.1016/j.heliyon.2024.e28365
Received 6 November 2023; Received in revised form 18 March 2024; Accepted 18 March 2024
Available online 19 March 2024

than 90% of the incidence types are ESCC [2,3]. ESCC progresses rapidly and is insensitive to chemotherapy, with more than 70% of patients dying within 5 years [4,5]. While current treatments do not provide a satisfactory prognosis, targeted therapy has recently been recognized as an exciting strategy for cancer treatment. However, no exciting therapeutic targets have been found in ESCC treatment. Therefore, research on the molecular mechanism of ESCC occurrence and development will help provide a new basis for ESCC treatment [6–8].

Aurora kinases (AURK) including AURKA, AURKB and AURKC, are serine/threonine kinases, which share a highly conserved catalytic autophosphorylation site [9]. AURKA promotes the progression of many cancers including bladder cancer, colorectal cancer, breast cancer, other solid tumors, and hematological malignancies [10–13]. AURKA is involved in various regulatory mechanisms in tumor tissues and is related to mitotic spindle formation [14]. In addition, AURKA can localize to the mitochondria to regulate mitochondrial dynamics and ATP production to influence tumor function [15]. A recent study found that AURKA can be localized in the nucleus to exert kinase-independent functions and affect tumor progression [16]. However, the mechanism of AURKA in ESCC remains unclear.

Ferroptosis, a unique type of cell death, results from iron-dependent phospholipid peroxidation. The Glutathione peroxidase 4 (GPX4)/glutathione (GSH)antioxidant system affects ferroptosis by regulating lipid peroxidation. Meanwhile, solute carrier family 7a member 11(SLC7A11) deficiency leads to GSH depletion [17,18]. Ferroptosis links metabolism, mitochondrial function, redox homeostasis, and human health. A study found that ferroptosis has great potential in tumor-related therapeutic processes [19]. The accumulation of oxidative stress in the mitochondria is the main process of ferroptosis, and AURKA can affect oxidative stress accumulation in the mitochondria in various cancers. However, whether AURKA affects oxidative stress accumulation in ESCC and whether it affects the process of ferroptosis are unknown. Therefore, this investigation was designed to explore the effect of AURKA and its specific mechanism in ESCC development and provide a new strategy for ESCC treatment.

2. Materials and methods

2.1. Bioinformatics analysis

The NCBI/GEO database (https://www.ncbi.nlm.nih.gov/geo/) was researched to retrieve expression profiles of patients with ESCC. GSE161533 and GSE149612 datasets were procured from the GEO database. The R language limma package was utilized for differential analysis of the GSE161533 probe data. RNA-sequencing analysis was performed on the GSE149612 dataset, and R language DESeq was used for the differential analysis. $P < 0.05$ and $|\log2FC| \geq 2$ were regarded as differential genes. The GEPIA (http://gepia.cancer-pku.cn/) was utilized

to scrutinize the expression levels of AURKA in ESCC and normal tissues.

2.2. Clinical tissue specimens

A collective assembly of 10 tumor tissues and corresponding 10 normal tissues were collected from 10 patients diagnosed with ESCC in 2022 at the Forth Hospital of Hebei Medical University. No irradiation or chemotherapy was administered to these patients before surgery. The tissue specimen includes the primary lesion tissue of ESCC and the corresponding adjacent normal tissue at a distance of 3–5 cm or more from the edge of the primary lesion. All specimens were fixed with formalin and embedded with paraffin.

Each individual patient provided written informed consent, and the research protocol was

Endorsed by the Ethics Committee of the Fourth Hospital, Hebei Medical University.

2.3. Cell culture

The human esophageal squamous cell carcinoma cell line Kyse150 was purchased from American Type Culture Collection (ATCC, VA, USA). Cultures are initiated in an RPMI-1640 (Invitrogen) medium complemented with 10 % volume heat-inactivated fetal bovine serum (Invitrogen). All cells were maintained in an atmosphere containing 5% CO_2 at 37 °C.

2.4. RNA extraction and quantitative real-time polymerase chain reaction (qRT-PCR) assay

According to the protocol, total RNA was isolated from ESCC cells utilizing the TRIzol reagent (Solarbio). The cDNA was synthesized in a reaction volume of 20 μL using the SureScript™ 1-Strand cDNA Synthesis Kit (GeneCopoeia, Inc.). The qRT-PCR reaction was executed using BlazeTaq™ SYBR® Green qPCR Mix 2.0 (GeneCopoeia, Inc.), operated in conjunction with the StepOne Plus Real-Time PCR System (Applied Biosystems). Glyceraldehyde-3-phosphate dehydrogenase (GAPDH) was utilized as an intrinsic control for

Table 1
Primers used for qRT-PCR.

Names	Sequences
AURKA	F: AAGACTTGGGTCCTTGGGTC R: CAAAGGAATGCGCTGGGAAG

F: Forward primer; R: Reverse primer.

mRNA using the $2^{-\triangle\triangle Ct}$ method [20]. Each specimen was tested in triplicate. Primer sequences used for qRT-PCR are listed in Table 1, including GAPDH and AURKA.

2.5. Cell transfection and treatment

The AURKA siRNA was purchased from GenePharma (Shanghai, China). The sequences are presented in Table 2. Lipofectamine 2000 Reagent (Invitrogen) was utilized for the transfection of cells that reached 70%–80% confluence. Transfection efficiency was assessed via quantitative real-time PCR analysis. The inhibitor, Fer-1, was purchased from MCE, and cells were treated at a final concentration of 8 ng/μL after transfection of si-AURKA.

2.6. Cell proliferation assay

The proliferative potential of the cell population was assayed via a Cell Counting Kit-8 (CCK8) methodology. Following a period of 24 h post transfection, the cells were harvested and transferred to the 96-well plate with 1×10^3 cells per well suspended in 100 μL 10 % fetal bovine serum. The final concentration of the iron inhibitor treatment group was 8 ng/μL. At 0, 24, 48, 72, and 96 h of incubation, 10 μL of the CCK8 (Boster) were respectively added to each well and left to incubate for a duration of 2 h. The optical density was detected utilizing a microplate reader (Thermo Fisher Scientific) at an optical absorbance wavelength of 450 nm for each well.

2.7. Flow cytometry assay

The cell cycle was measured by flow cytometry. Following a period of 48–72 h post-transfection, the cells were harvested, meticulously washed with chilled phosphate-buffered saline (PBS), and then fixed with 70% ethanol at 4 °C for an extended period of overnight. Then cells were stained with propidium iodide staining solution (Beyotime). Samples were then maintained in the absence of light for a period of 30 min. Through detecting the fluorescence of propidium iodide inside the cell, the amount of DNA content inside the cell can be determined. The cell cycle enters G1, S, G2, and M phases from G0 phase, and the cell DNA content also changes from diploid to tetraploid. Therefore, the cell cycle can be determined by detecting the cell DNA content using the flow cytometry assay [21].

2.8. Transwell migration and invasion assay

Cell Invasion and metastasis ability were detected by Transwell assay. The transwell migration assay was performed using non-Matrigel-coated chambers (Coring). After 24 h of transfection, 1×10^5 cells, suspended in 200 μL of serum-free 1640 medium, were relocated to the upper chamber of the chamber apparatus, and 600 μL of 10% fetal bovine serum was positioned in the lower chamber. After 24 h of incubation at 37 °C and 5% CO_2, cells on the inferior aspect of the membrane were affixed with 4% paraformaldehyde and counterstained with crystal violet solution. The transwell invasion assay was conducted as above, except that the upper chamber was coated with 50 μL of Matrigel (Corning). The count of cells on the inferior membrane was evaluated utilizing a microscope.

2.9. Immunohistochemistry (IHC) assay

For the IHC assay, slides were deparaffinized in xylene at 56 °C overnight followed by dehydration in alcohol stages. The paraffin sections were hydrated and antigen-retrieved with the EDTA repair solution at 100 °C for 15 min. After 30 min of chilling at room temperature, the slides were exposed to 3% hydrogen peroxide for 20 min, inhibiting endogenous peroxidase activity. Then, the nonspecific binding sites were blocked with 10% goat serum at room temperature for 45 min. Anti-AURKA (Ab13824, abcam), anti-Ki67 (A00254, Boster), and anti-vimentin (PB9359, Boster) were used to incubate with the slides at 4 °C overnight. After washing with PBS, the horseradish-peroxidase (HRP)-conjugated secondary antibody was used to incubate with the slides for 1 h. Then, the slides were cleansed with PBS, the 3,3-diaminobenzidine solution was administered at ambient temperature. Ultimately, the slides were counterstained with hematoxylin, dehydrated through sequential stages of alcohol, and affixed. The expression levels of AURKA, Ki67, and vimentin were evaluated according to the degree and intensity of staining [22].

2.10. Hematoxylin eosin (HE) staining

Tumors underwent fixation with 4% paraformaldehyde for 24 h, then paraffin embedding. Subsequently, 5 μm sections placed onto

Table 2
Primers used for siRNA.

Names	Sequences
si-AURKA	F: GGACCUGUUAAGGCUACAGTT R: CUGUAGCCUUAACAGGUCCTT

F: Forward primer; R: Reverse primer.

microslides, were stained by the HE staining kit (ZSGB-BIO) according to the protocol.

2.11. Western blot assay

For protein extraction, cells were processed with RIPA (Solarbio) and PMSF (Sigma-Aldrich). The protein concentration was determined using a BCA Kit (Beyotime). Proteins were separated by 10% sodium dodecyl sulfate-polyacrylamide gel electrophoresis (SDS-PAGE) at 80V and transferred to the polyvinylidene difluoride membrane (Millipore) at 200 mA. Following protein blocking with 5% skim milk, the membrane was incubated for 1 h at room temperature. Antibodies against AURKA 1:1000 (Ab13824, abcam), SLC7A11 1:2000 (BM5318, Boster), GAPDH 1:5000 (60004-1-Ig, proteintech), and GPX4 1:2000 (BM5231, Boster) was added to incubate with the membrane at 4 °C overnight. After membrane was wash with TBS-T three times, the secondary antibody (BM2020, Boster 1:2000) was then added to incubate with Membrane incubation at room temperature for 2 h. The protein bands were detected by Chemi XT 4 (Syngene) using the enhanced chemiluminescence detection reagent (Multisciences, Biotech Co., Ltd).

2.12. Iron ion kit

Sample preparation: Each group of cells received two washes with 2 mL PBS. Cells subjected to a lysis reaction using 200 μL/well lysis buffer, shaking for 2 h. Gradient dilution of the samples was was conducted as kit protocol, and solution A was mixed: the buffer was mixed with 4.5% potassium permanganate solution at 1:1, and the blank control tube, standard tube, si-NC tube, and si-AURKA tube were added. The sample was mixed well, Incubated at 60 °C for 1 h, then cooled to room temperature. vortexed for 5 s, 30 μL of iron ion detection reagent were added and thoroughly mixed, followed by incubation at ambient temperature for 30 min, and centrifuged to take the supernatant. Then, A volume of 200 μL was transferred to a 96-well plate for absorbance measurement at 550 nm. A standard curve was drawn and iron ion concentration was calculated.

2.13. GSH kit

Sample preparation: Each group of treated cells were collected by centrifugation into a centrifuge tube, 1 mL of the reagent was added to process the samples, sonicated in an Icing bath, and Centrifugation at 8000*g* for 10 min at 4 °C, followed by supernatant collection. Preparation of the standard diluent: The 10 mg/mL GSH standard solution was diluted using the diluent following the instructions for the standard diluent. Reagent 2 was preheated at 37 °C for 30 min before use: reagent 2, 700 μL, reagent 3, 200 μL, si-NC tube and si-AURKA tube, 100 μL each. Standard tube: reagent 2, 700 μL, reagent 3, 200 μL, standard diluent, 100 μL; Blank tube: reagent 2, 700 μL, reagent 3, 200 μL, and distilled water, 100 μL. These were mixed well, until color developed for 2 min at room temperature. Then, 200 μl of template was loaded into a 96-well plate, with absorbance determined at 412 nm. A standard curve was drawn, and GSH concentrations were calculated.

2.14. MDA kit

In each group, cells were collected by centrifugation, and an appropriate amount of extract was added for sonication, centrifuged at 8000 g for 10 min at 4 °C, and the supernatant was taken for testing according to kit instructions. The measuring and blank tubes were arranged according to the instructions, and cells were bathed in boiling water for 60 min. The sample was refrigerated to room temperature, then centrifuged at 10,000 g for 10 min, extracting the supernatant, and the MDA concentration of each group was calculated according to the instructions.

2.15. Tumor xenograft model

The animal experiments were approved by the Ethics Committee of the Animal Experiments of the Fourth Hospital of Hebei Medical University and in accordance with the guidelines of NIH. These mice were kept in the IVC system animal room. Fifteen female BALB/c-nude mice aged 6–8 weeks, sourced from Sperford Biotechnology Co., Ltd, were randomized into three groups of si-NC ($n = 5$), si-AURKA ($n = 5$), and si-AURKA + Fer-1 (8 ng/μL) ($n = 5$). A total of 5×10^6 Kyse150 cells stably transfected with si-NC and si-AURKA suspended in 200 μL PBS were inoculated in the subcutaneous forelimb armpit of each mouse. Tumor weights were assessed for 3 weeks Tumor tissue was used to make paraffin sections for HE staining and IHC 3 weeks later.

2.16. Statistical analysis

The results were analyzed by SPSS Statistics for Windows v22.0 (IBM Corp., Armonk, NY, USA) and GraphPad Prism 8, and data were presented as mean ± standard deviation. Differences significant between the two groups were evaluated via a Student's t-test, and a one-way analysis of variance was conducted among three or more groups. All experiments were conducted independently in triplicate, and statistical significance was set at $P < 0.05$.

3. Results

3.1. AURKA was a differential gene and highly expressed in tumor tissues of ESCC

RNA-sequencing analysis was performed on the GSE149612 dataset, and a total of 1917 downregulated and 2010 upregulated genes were screened (Fig. 1A and B). We analyzed GSE161533 datasets, and uncovered a total of 9283 genes, with 4230 down-regulated gene and 5053 upregulated genes (Fig. 1C and D). A total of 2278 co-expressed genes were found, and AURKA is an upregulated differential gene shared by both databases (Fig. 1E). Moreover, the expression of AURKA in esophageal cancer tissues was observed via the GEPIA database (Fig. 1F). In this research, IHC showed that AURKA upregulated in clinical tumor tissues (Fig. 1G) ($P = 0.0073$), which further verified the accuracy of sequencing data.

3.2. Interference with AURKA inhibits ESCC cell proliferation, invasion, migration, and cell cycle

Then, the impact of AURKA on the biological conduct of Kyse150 cells was examined. AURKA's relative expression was

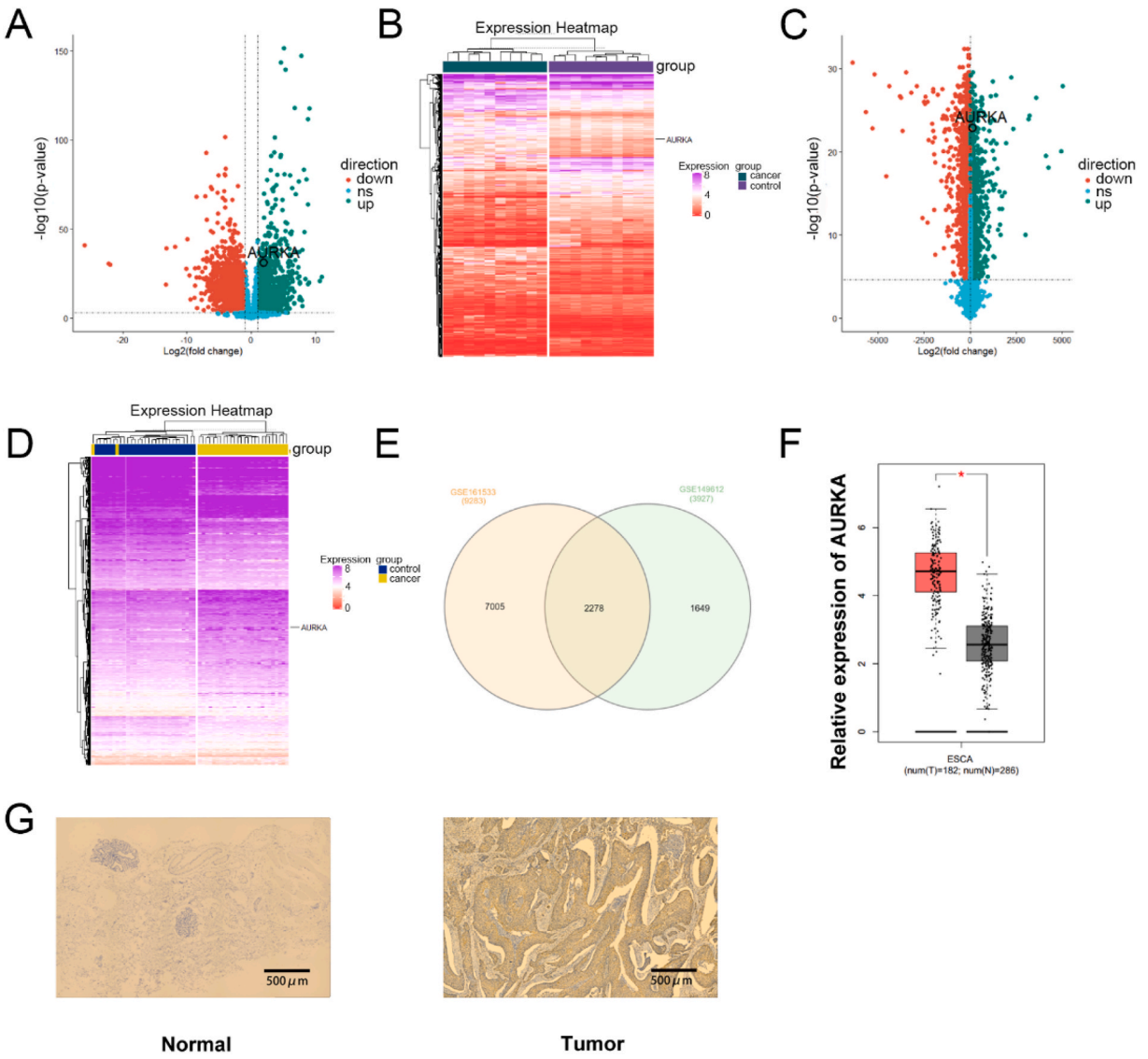

Fig. 1. AURKA is a differential gene and is highly expressed in tumor tissues of esophageal squamous cell carcinoma (ESCC) according to the GEO databases. **(A)** Volcano plot of expression between tumor tissues and normal tissues of ESCC in GSE149612. **(B)** Expression heat map between tumor tissues and normal tissues in GSE149612. **(C)** Volcano plot of expression between tumor tissues and normal tissues in GSE161533. **(D)** Expression heat map between tumor tissues and normal tissues in GSE161533. **(E)** Venn diagram of GSE161533 and GSE149612 differential genes. **(F)** Expression of AURKA in esophageal cancer in GEPIA database. **(G)** Immunohistochemistry of normal and tumor tissue of ESCC. Scale bar: 500 μm.

considerably downregulated in the si-AURKA group versus control group data (0.50 ± 0.10 vs 1.00 ± 0.01, $P = 0.0010$) (Fig. 2A). CCK8 results showed that proliferation ability was decreased in Kyse150 cells with si-AURKA (Fig. 2B). According to the flow cytometry analysis, AURKA inhibition leads to a prolongation of the G2 phase (24.10 ± 1.21 vs 18.00 ± 2.71, $P = 0.0235$), an increase of cells in the S phase (30.90 ± 0.36 vs 16.70 ± 2.04, $P = 0.0003$), and reduction of cells in the G1 phase (45.00 ± 1.49 vs 65.30 ± 4.48, $P = 0.0017$) (Fig. 2C), which also indicated the proliferation promotion effect of AURKA on ESCC cells. The transwell migration

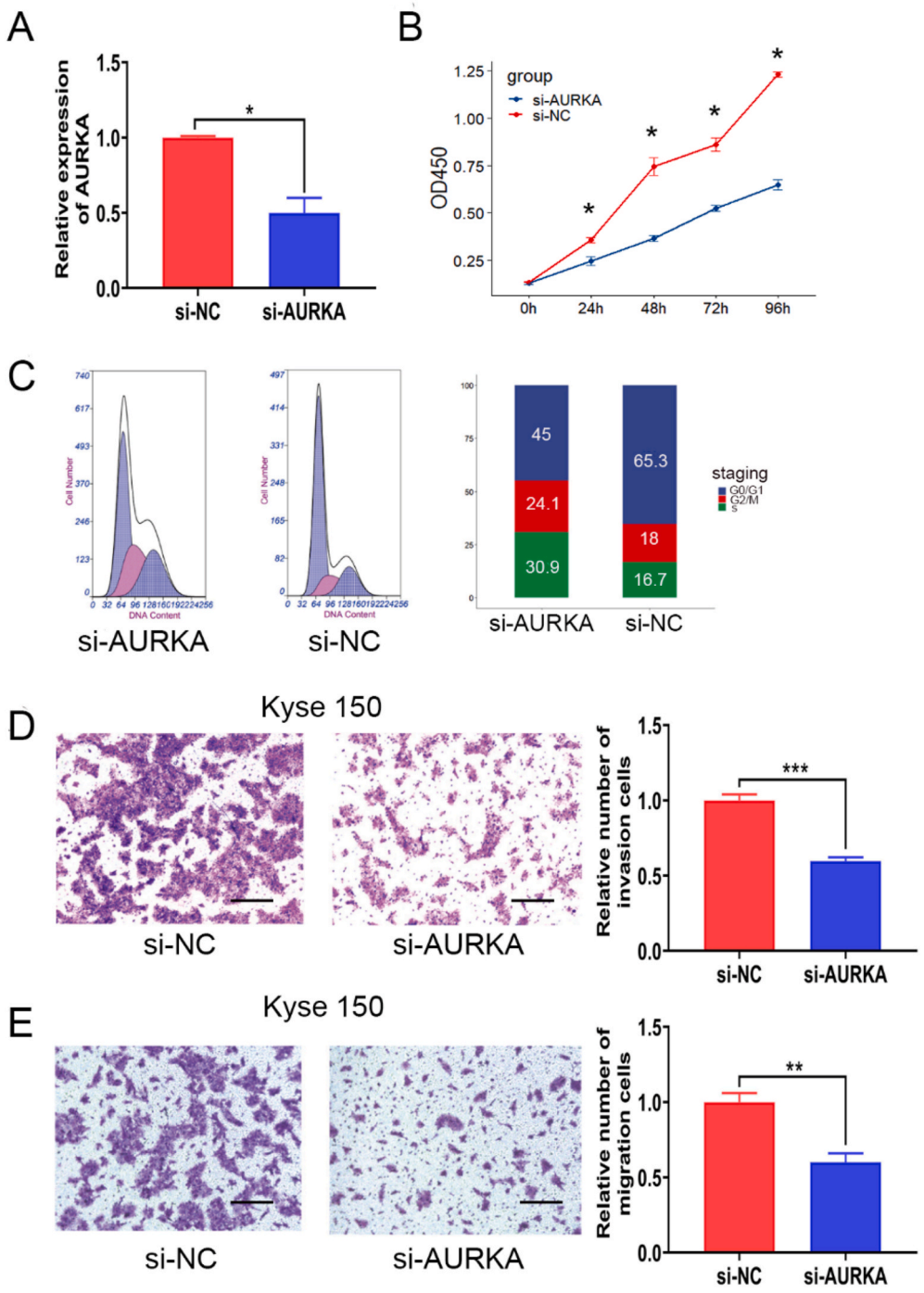

Fig. 2. Knockdown of AURKA suppresses cell proliferation, migration, and invasion of ESCC cells. **(A)** The knockdown efficiency of AURKA detected by qRT-PCR method. **(B)** The cell proliferation ability was assessed by CCK8 assay in Kyse150 cells with AURKA knockdown. **(C)** The Flow cytometry assay was performed to evaluate the cell cycle in AURKA knockdown Kyse150 cells. **(D, E)** Transwell assays were conducted to measure the migration and invasion ability after inhibition of AURKA in Kyse150 cells (magnification: × 100). *$P < 0.05$. **$P < 0.01$. ***$P < 0.001$.

and invasion assays demonstrated that the migration (0.60 ± 0.06 vs 1.00 ± 0.06, $P = 0.0012$) and invasion (0.59 ± 0.03 vs 1.00 ± 0.04, $P = 0.0001$) abilities of Kyse150 cells were remarkably weakened as to the AURKA knockdown (Fig. 2D and E).

3.3. AURKA affects ferroptosis

To explore the possible mechanism of AURKA in affecting esophageal cancer progression, we found that in Kyse150 cells, Iron levels in the si-AURKA group were elevated compared to those in the si-NC group (2.54 ± 0.27 vs 1.78 ± 0.32, $P = 0.0350$) (Fig. 3A). However, the ferroptosis-protective glutathione was downregulated (0.06 ± 0.002 vs 0.14 ± 0.004, $P < 0.0001$) (Fig. 3B), and the MDA content was increased (0.00078 ± 0.000035 vs 0. 00033 ± 0.000045, $P = 0.0002$) (Fig. 3C). These findings suggest that ferroptosis in the AURKA knockdown group was enhanced. Furthermore, the expression levels of GPX4 (0.18 ± 0.05 vs 1.07 ± 0.09, $P = 0.0001$) and SLC7A11 (0.15 ± 0.10 vs 0.90 ± 0.25, $P = 0.0080$) were detected using Western blot assay, results showed a reduction in the AURKA knockdown group (0.46 ± 0.23 vs 1.11 ± 0.30, $P = 0.0377$), and the difference was statistically significant (Fig. 3D–G).

3.4. Effect of co-transfection of si-AURKA and Fer-1 on the biological function of ESCC cells

Given that AURKA may play an oncogene role by participating in ferroptosis-related signaling pathways,and the effect of ferroptosis inhibitor Fer-1 on the biological behavior of ESCC cells was further explored with AURKA inhibition. Transwell invasion assay results indicated that si-AURKA treatment significantly suppressed cell invasion (0.46 ± 0.03 vs 1.00 ± 0.08, $P < 0.0001$) compared with those in the si-NC group, However, Fer-1 partly reversed AURKA's suppressive influence on cell invasion (0.66 ± 0.02 vs 0.46 ± 0.03, $P = 0.0057$) (Fig. 4A). Transwell migration assay outcomes indicated that cells in the si-AURKA group (0.35 ± 0.03 vs 1.00 ± 0.03, $P < 0.0001$) were decreased comparing to those in si-NC, and Fer-1 partly reversed AURKA's suppressive influence on cell

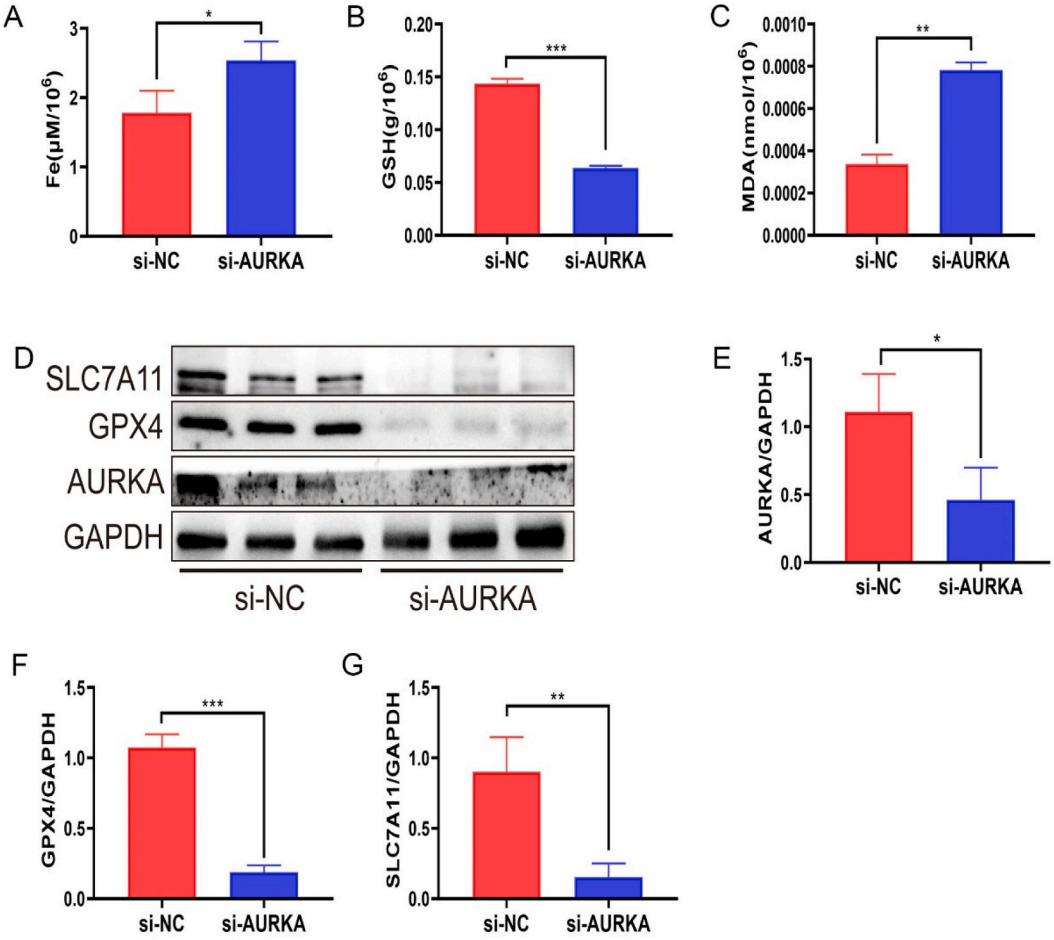

Fig. 3. The relationship between AURKA and the ferroptosis process **(A–C)** Changes of ferroptosis detected by the expression of Fe (A), GSH (B), MDA (C) in si-AURKA group and si-NC group in Kyse150 cells. **(D)** Expression of AURKA, GPX4, SLC7A11 in si-AURKA group and si-NC group in Kyse150 cells. Original western blots were presented in Supplementary Fig. 1. **(E-G)** Histogram of AURKA (E), GPX4 (F), SLC7A11 (G) expression. *$P < 0.05$. **$P < 0.01$. ***$P < 0.001$.

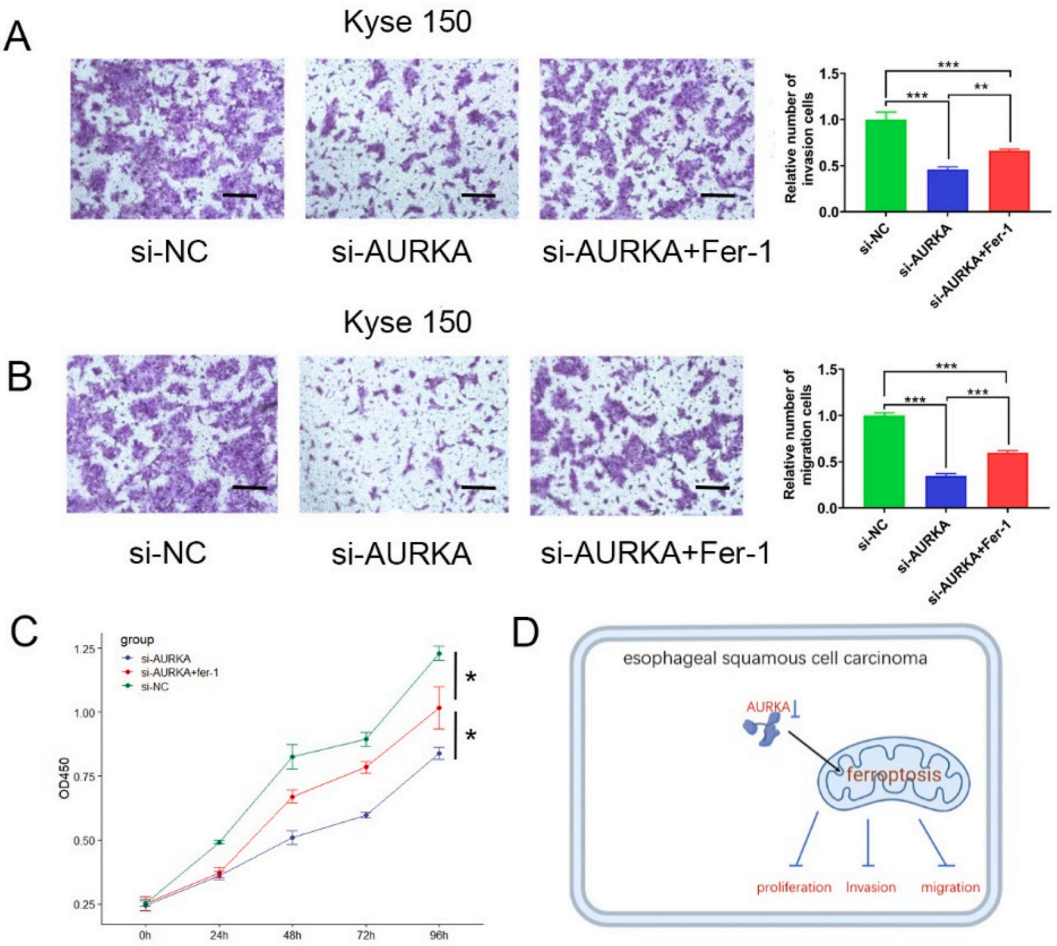

Fig. 4. Functional rescue experiment after co-intervention of si-AURKA and Ferrostatin-1 (Fer-1). **(A, B)** The transwell migration and invasion assays were performed following treated with Fer-1 in the AURKA knockdown group in Kyse150 cells (magnification: × 100). **(C)** CCK8 assay was rescued by Fer-1 intervention in AURKA knockdown cells. **(D)** The graphic abstract that AURKA promotes ESCC proliferation, migration, and invasion by inhibiting ferroptosis. *$P < 0.05$. **$P < 0.01$. ***$P < 0.001$.

migration (0.60 ± 0.02 vs 0.35 ± 0.03, $P < 0.0001$) (Fig. 4B). The CCK8 assay demonstrated that cell proliferation ability could be also partially reversed in the Fer-1 treated group compared with that in the si-AURKA group (Fig. 4C). Therefore, AURKA may inhibit ferroptosis to influence ESCC cell proliferation, migration, and invasion (Fig. 4D).

3.5. AURKA knockdown suppresses ESCC growth in vivo, and Fer-1 partially reverses this effect

To assess AURKA's role in esophageal squamous cell carcinoma in vivo, si-NC and si-AURKA that can be used for stably transfected ESCC cells were used, and the result of qRT-PCR revealed that siRNAs could significantly decrease the expression level of AURKA (Fig. 5A). si-AURKA-2, which exhibited the most evident knockdown efficacy, was selected for the transfection of Kyse150 cells. Then, nude mice with Kyse150 cells that were stably transfected with si-AURKA were inoculated. In the analysis of the tumor weight and morphology, AURKA knockdown (1.910 ± 0.054 *vs* 2.130 ± 0.097, $P = 0.0011$) significantly reduced tumor growth in mice, whereas Fer-1 partially reversed this effect (2.042 ± 0.058 vs 1.910 ± 0.054, $P = 0.0339$) (Fig. 5B and C). HE staining results indicated that tumor cells had disordered distribution, abnormal shapes, with heavily stained cytoplasm in the control group, and these pathological changes were lighter in the si-AURKA group; furthermore, AURKA, Ki-67, and vimentin levels in subcutaneous tumors formed by AURKA knockdown in Kyse150 cells, as judged by IHC, were less than those in the control group. However, the HE staining change in tumor cells and expression changes in AURKA, Ki-67, and vimentin were partially restored in the Fer-1 group (Fig. 5D). These results showed that interference with AURKA inhibited the growth of ESCC in vivo; however, Fer-1 may reverse this effect to a certain extent.

4. Discussion

Recent studies have found that AURKA is closely associated with tumor progression, platinum resistance, and other biological

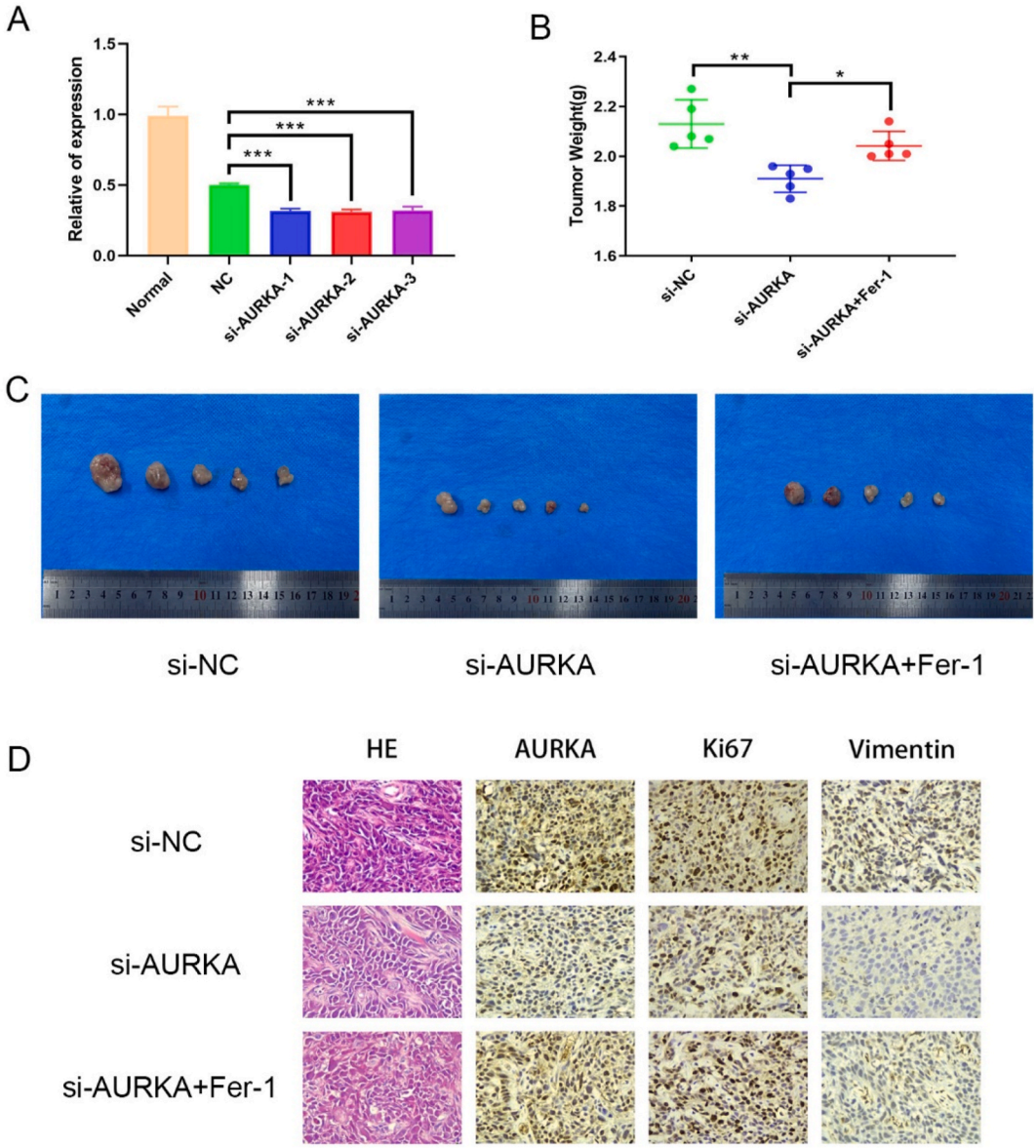

Fig. 5. Interference with AURKA suppresses ESCC growth in vivo, and Fer-1 partially reverses this effect **(A)** The interfering efficiency against AURKA analyzed by qRT-PCR method. **(B)** The tumor weight was shown. **(C)** Photographs of xenograft tumors formed by Kyse150 cells stably transfected with si-NC, si-AURKA, and Fer-1 pretreatment. **(D)** HE staining was used to reveal the tissues of the subcutaneous tumors, and IHC was performed to evaluate the expression of AURKA, Ki67, and Vimentin in the subcutaneous tumors (magnification: × 400). $^{*}P < 0.05$. $^{**}P < 0.01$. $^{***}P < 0.001$.

processes [23,24]. however, the mechanism of AURKA in ESCC is still unclear. Initially, we analyzed the RNA-seq and microarray information of ESCC in the GEO database and found that AURKA was a differential gene and increased in tumor tissues. Therefore, AURKA may serve as an oncogene in ESCC. IHC assay showed that AURKA was upregulated in tumor tissues, which was consistent with the bioinformatics analysis of the database. To confirm whether AURKA affects the pathological process of ESCC, AURKA was knocked down from cells and the malignant behavior of Kyse150 cells were significantly inhibited by AURKA knockdown.

Ferroptosis, as a new necrosis type, driven by iron-dependent lipid peroxidation [25], is different from apoptosis, necroptosis, and pyroptosis [26]. Therapeutics targeting ferroptosis mechanism have been discovered in many cancer trials in vitro and in vivo [27–29]. Sorafenib inhibits GSH production through inhibiting system x_c^-, thus promoting ferroptosis [30]. In colon cancer and NSCLC, cisplatin triggers ferroptosis by GSH depletion and GPX4 inactivation [31]. In particular, it has been reported that, by triggering cell ferroptosis, metronomic capecitabine therapy demonstrated efficacy and safety in hepatocellular carcinoma (HCC) patients who are resistent to first-line sorafenib [32]. Ferroptosis provides a new idea for tumor treatment and opens a new way for clinical treatment.

Ferroptosis induces mitochondrial fragmentation, mitochondrial reactive oxygen species (ROS) production, loss of mitochondrial

membrane potential, and ATP depletion [25]. AURKA knockdown substantially enhanced mitochondrial ROS production in oral squamous cell carcinoma cells [33]. GPX4 was thought to be the main enzyme that prevents ferroptosis [34]. Gomaa et al. [35] found that AURKA inhibition or miR-4715-3p reconstitution in gastric cancer suppressed GPX4 and induced cell death. Therefore, we speculate whether AURKA exerts an antitumor effect by influencing ferroptosis. In this study, ferroptosis-related kits such as MDA, Fe, and GSH were measured. The expression levels of MDA and Fe in the si-AURKA group were considerably increased, whereas that of GSH, the protective substance, decreased. SLC7A11 or GPX4 inhibition can trigger ferroptosis [36]. In the Western blot assay, levels of GXP4 and SLC7A11 in the si-AURKA group were significantly decreased. All these results suggest that ferroptosis is enhanced after AURKA knockdown in ESCC. To further verify our hypothesis, we applied Fer-1, an inhibitor of ferroptosis, after AURKA knockdown in Kyse150 cells, and cell proliferation, invasion, and metastasis abilities were restored. The in vivo study on nude mice also confirmed this point of view. The tumors in the si-NC and Fer-1 groups were larger than that in the si-AURKA group, and the IHC results also revealed that proliferation- and metastasis-related biomarkers in the Fer-1 group were restored. Therefore, AURKA may affect ESCC progression through ferroptosis.

According to Baocong Shan [37], AURKA knockdown resulted in TP53 upregulation and phosphorylated TP53 downregulation in colon cancer cells, affecting oxaliplatin sensitivity. Meanwhile, p53 can enhance ferroptosis through the inhibition of SLC7A11 expression or promotion of spermidine/spermine N1-acetyltransferase 1 (SAT1) and glutaminase 2 (GLS2) expression. Thus, AURKA might affect biological processes of ESCC by affecting p53 and then influencing ferroptosis [38]. However, the specific regulatory mechanism of AURKA on ferroptosis must be further studied.

In conclusion, the present findings indicate that AURKA knockdown could inhibit the proliferation, invasion, and metastasis of ESCC in vivo and in vitro, and AURKA may affect ESCC progression via ferroptosis. These findings may provide a new reference for cancer-targeted therapy in ESCC.

Ethics statement

The animal experiments were approved by the Ethics Committee of the Animal Experiments of the Fourth Hospital of Hebei Medical University and in accordance with the guidelines of NIH, and the approval number was 2022059.

Funding

This work was supported by Grants from the Major Projects of Hebei Provincial Science and Technology Department (No. 22377769D) and Hebei Province annual medical science research project (No. 20240625).

Data availability statement

The data sets scrutinized throughout the current investigation are available from the corresponding author upon reasonable request.

CRediT authorship contribution statement

Yuan Mi: Writing – original draft, Software, Methodology, Conceptualization. **Liying Chen:** Writing – original draft, Methodology, Data curation, Conceptualization. **Cong Wang:** Methodology, Conceptualization. **Yuxin Miao:** Methodology, Conceptualization. **Chuntao Song:** Formal analysis, Data curation. **Jie Su:** Formal analysis, Data curation. **Lei Wang:** Writing – review & editing, Funding acquisition, Conceptualization.

Declaration of competing interest

The authors declare that they have no known competing financial interests or personal relationships that could have appeared to influence the work reported in this paper.

Acknowledgments

We would like to thank Prof. Liang Liu (The Fourth Hospital of Hebei Medical University, Shijiazhuang, China) for kindly providing a laboratory site.

Appendix A. Supplementary data

Supplementary data to this article can be found online at https://doi.org/10.1016/j.heliyon.2024.e28365.

References

[1] Y. Li, Y. Li, X. Chen, NOTCH and esophageal squamous cell carcinoma, Adv. Exp. Med. Biol. 1287 (2021) 59–68.
[2] Y. Cui, et al., RNA m6A demethylase FTO-mediated epigenetic up-regulation of LINC00022 promotes tumorigenesis in esophageal squamous cell carcinoma, J. Exp. Clin. Cancer Res. 40 (1) (2021) 294.
[3] X. Hu, et al., circGSK3beta promotes metastasis in esophageal squamous cell carcinoma by augmenting beta-catenin signaling, Mol. Cancer 18 (1) (2019) 160.
[4] A. Pennathur, et al., Oesophageal carcinoma, Lancet 381 (9864) (2013) 400–412.
[5] P.C. Enzinger, R.J. Mayer, Esophageal cancer, N. Engl. J. Med. 349 (23) (2003) 2241–2252.
[6] Y. Baba, et al., Tumor immune microenvironment and immune checkpoint inhibitors in esophageal squamous cell carcinoma, Cancer Sci. 111 (9) (2020) 3132–3141.
[7] L.Y. Chu, et al., Blood-based biomarkers for early detection of esophageal squamous cell carcinoma, World J. Gastroenterol. 26 (15) (2020) 1708–1725.
[8] W. Li, J. Liu, H. Zhao, Identification of a nomogram based on long non-coding RNA to improve prognosis prediction of esophageal squamous cell carcinoma, Aging (Albany NY) 12 (2) (2020) 1512–1526.
[9] R. Du, et al., Targeting AURKA in Cancer: molecular mechanisms and opportunities for Cancer therapy, Mol. Cancer 20 (1) (2021) 15.
[10] H. Zhen, et al., LINC00958 promotes bladder cancer carcinogenesis by targeting miR-490-3p and AURKA, BMC Cancer 21 (1) (2021) 1145.
[11] J. Tang, et al., ARID3A promotes the development of colorectal cancer by upregulating AURKA, Carcinogenesis 42 (4) (2021) 578–586.
[12] H.J. Donnella, et al., Kinome rewiring reveals AURKA limits PI3K-pathway inhibitor efficacy in breast cancer, Nat. Chem. Biol. 14 (8) (2018) 768–777.
[13] C.A. Moreira-Nunes, et al., Targeting aurora kinases as a potential prognostic and therapeutical biomarkers in pediatric acute lymphoblastic leukaemia, Sci. Rep. 10 (1) (2020) 21272.
[14] C. Shi, et al., Aurora kinase A inhibition induces synthetic lethality in SMAD4-deficient colorectal cancer cells via spindle assembly checkpoint activation, Oncogene 41 (19) (2022) 2734–2748.
[15] G. Bertolin, M. Tramier, Insights into the non-mitotic functions of Aurora kinase A: more than just cell division, Cell. Mol. Life Sci. 77 (6) (2020) 1031–1047.
[16] F.D. Naso, et al., Nuclear localisation of Aurora-A: its regulation and significance for Aurora-A functions in cancer, Oncogene 40 (23) (2021) 3917–3928.
[17] T. Xu, et al., Molecular mechanisms of ferroptosis and its role in cancer therapy, J. Cell Mol. Med. 23 (8) (2019) 4900–4912.
[18] D. Li, Y. Li, The interaction between ferroptosis and lipid metabolism in cancer, Signal Transduct. Targeted Ther. 5 (1) (2020) 108.
[19] Z. Ye, et al., FBW7-NRA41-SCD1 axis synchronously regulates apoptosis and ferroptosis in pancreatic cancer cells, Redox Biol. 38 (2021) 101807.
[20] K.J. Livak, T.D. Schmittgen, Analysis of relative gene expression data using real-time quantitative PCR and the 2(-Delta Delta C(T)) Method, Methods 25 (4) (2001) 402–408.
[21] J. Wang, et al., SRSF1-dependent alternative splicing attenuates BIN1 expression in non-small cell lung cancer, J. Cell. Biochem. 121 (2) (2020) 946–953.
[22] Y. Jia, et al., Low expression of Bin1, along with high expression of Ido in tumor tissue and draining lymph nodes, are predictors of poor prognosis for esophageal squamous cell cancer patients, Int. J. Cancer 137 (5) (2015) 1095–1106.
[23] L. Wang, et al., Cisplatin-resistant cancer cells are sensitive to Aurora kinase A inhibition by alisertib, Mol. Oncol. 11 (8) (2017) 981–995.
[24] Z. Shen, et al., Combined inhibition of AURKA and HSF1 suppresses proliferation and promotes apoptosis in hepatocellular carcinoma by activating endoplasmic reticulum stress, Cell. Oncol. 44 (5) (2021) 1035–1049.
[25] C.M. Bebber, et al., Ferroptosis in cancer cell biology, Cancers 12 (1) (2020).
[26] Z. Ye, et al., Ferroptosis: final destination for cancer? Cell Prolif. 53 (3) (2020) e12761.
[27] K. Wang, et al., Branched-chain amino acid aminotransferase 2 regulates ferroptotic cell death in cancer cells, Cell Death Differ. 28 (4) (2021) 1222–1236.
[28] S. Ma, et al., Ferroptosis is induced following siramesine and lapatinib treatment of breast cancer cells, Cell Death Dis. 7 (7) (2016) e2307.
[29] V.E. Kagan, et al., Oxidized arachidonic and adrenic PEs navigate cells to ferroptosis, Nat. Chem. Biol. 13 (1) (2017) 81–90.
[30] S.J. Dixon, et al., Pharmacological inhibition of cystine-glutamate exchange induces endoplasmic reticulum stress and ferroptosis, Elife 3 (2014) e02523.
[31] J. Guo, et al., Ferroptosis: a novel anti-tumor action for cisplatin, Cancer Res Treat 50 (2) (2018) 445–460.
[32] H. Wang, et al., Metronomic capecitabine with rapamycin exerts an immunosuppressive effect by inducing ferroptosis of CD4(+) T cells after liver transplantation in rat, Int. Immunopharm. 124 (Pt A) (2023) 110810.
[33] H. Dawei, D. Honggang, W. Qian, AURKA contributes to the progression of oral squamous cell carcinoma (OSCC) through modulating epithelial-to-mesenchymal transition (EMT) and apoptosis via the regulation of ROS, Biochem. Biophys. Res. Commun. 507 (1–4) (2018) 83–90.
[34] K. Bersuker, et al., The CoQ oxidoreductase FSP1 acts parallel to GPX4 to inhibit ferroptosis, Nature 575 (7784) (2019) 688–692.
[35] A. Gomaa, et al., Epigenetic regulation of AURKA by miR-4715-3p in upper gastrointestinal cancers, Sci. Rep. 9 (1) (2019) 16970.
[36] W. Zhang, et al., RBMS1 regulates lung cancer ferroptosis through translational control of SLC7A11, J. Clin. Invest. 131 (22) (2021).
[37] B. Shan, et al., AURKA increase the chemosensitivity of colon cancer cells to oxaliplatin by inhibiting the TP53-mediated DNA damage response genes, BioMed Res. Int. 2020 (2020) 8916729.
[38] R. Kang, G. Kroemer, D. Tang, The tumor suppressor protein p53 and the ferroptosis network, Free Radic. Biol. Med. 133 (2019) 162–168.